Continuous-wave operation of a 5.2 μm quantum-cascade laser up to 210 K

Brian Ishaug,[a] Wen-Yen Hwang, Jae Um, Bujin Guo, Hao Lee, and Chih-Hsiang Lin
Applied Optoelectronics Inc., 13111 Jess Pirtle Boulevard, Sugar Land, Texas 77478

(Received 29 March 2001; accepted for publication 13 July 2001)

Continuous-wave operation of a 5.2 μm-type I quantum-cascade laser with more than 5 mW of output power is reported at a heat sink temperature of 210 K (-63 °C). This temperature is within the range obtainable with thermal-electric coolers. The device was mounted epi-side down on a copper submount and exhibited a thermal resistance of ~10 K/W at 210 K. Using the experimentally determined values for $T_0=136$ K, $J_0=535$ A/cm^2 and $V_{op}=8.1$ V and the above thermal resistance, the maximum theoretical operating temperature was found to be 212 K, in close agreement with experiment. Thermal simulations show that by improving the device design and heat sinking, thermal resistance can be reduced to 8.8 K/W and the maximum cw operating temperature can be increased to 230 K. © *2001 American Institute of Physics.* [DOI: 10.1063/1.1402644]

Mid-infrared (MIR) lasers are highly desirable for a variety of applications such as medical diagnostics, remote chemical sensing (CO, HF, CH_4, C_2H_6, HCl, CO_2, N_2O, O_3, etc.) and molecular spectroscopy. However, MIR systems are limited by a lack of adequate MIR sources. Conventional MIR sources such as solid-state lasers and optical parametric oscillators are expensive and difficult to use. Semiconductor diode lasers, on the other hand, have significant advantages in terms of cost, volume, weight, reliability, and power dissipation. A compact, MIR semiconductor laser would be extremely useful for many of the above applications.[1] InGaAs/InAlAs-type I quantum-cascade (QC) lasers are promising candidates in the wavelength range from 3.4 to 17 μm. Above room temperature operation of Fabry-Pérot and distributed feedback QC lasers in pulsed mode at 5.4 and 8 μm[2,3] clearly shows the viability of these devices. However, for the ultimate in sensitivity and spectral resolution, continuous wave (cw) operation is desired but, because of active region heating, cw operation is typically limited to cryogenic temperatures. Recent advances, however, show that near room temperature cw operation is possible at long wavelengths, >7 μm.[4,5] In this letter we report cw operation of a 5.2 μm QC laser at 210 K and show that with improved device design and heat sinking, operation up to 230 K is feasible.

The InAlAs/InGaAs/InP QC laser reported in this letter was grown in a Riber 32P molecular beam epitaxy system using elemental In, Ga, Al, and Si. P_2 and As_2 were supplied via solid phosphorous and arsenic valved sources. X-ray diffraction measurements were used to determine the material composition and the layer thickness. The laser structure consisted of a 0.425 μm InGaAs bottom confinement layer, a 26-stage InGaAs/InAlAs active region, a 0.525 μm InGaAs top confinement layer, a 2.81 μm InP top cladding layer, and a 0.02 μm n^+ InGaAs contact layer on an n^+ InP substrate. Each stage in the active region consisted of a modulation doped tunneling injector followed by a three-quantum-well vertical transition photon emitter region. [6] The laser wafer was processed into 12-μm-wide by 5-μm-tall mesa-confined narrow stripe lasers with cavity lengths of 2 mm.

Following cleaving and dicing, the device was mounted epi-side down on a copper submount and then secured to a cryostat cold finger. The temperature of the cold finger was measured using a pair of silicon diodes to insure accuracy. Continuous wave light output (L) versus current input (I) measurements as well as voltage (V) versus current (I) measurements were performed on the device at various heat sink temperatures between 80 and 210 K. The $L-I$ curves along with a representative $I-V$ curve taken at 210 K are shown in Fig. 1.

From the slope of the $L-I$ curve at 80 K, the external quantum efficiency of this device was found to be as high as 350% and the maximum output power at 210 K was more than 5 mW. The $L-I$ curves at low temperatures are only shown to certain injection currents due to the limited heat

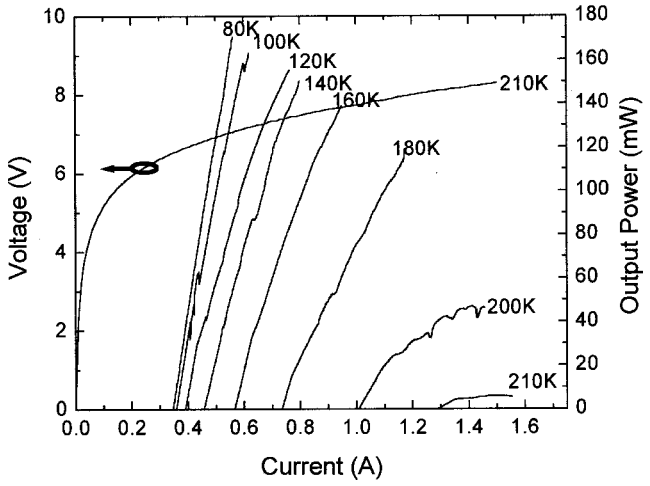

FIG. 1. Steady state cw light output (L) versus current (I) at various heat sink temperatures. The measured output power from a single facet is multiplied by 2 to account for output from both facets and corrected by a factor of 1.4 to account for the 70% collection efficiency giving the total output power as indicated in the graph. The noise in the data is mostly from spatial mode hopping. The $I-V$ curve shown was taken at 210 K.

[a]Electronic mail: bishaug@ao-inc.com

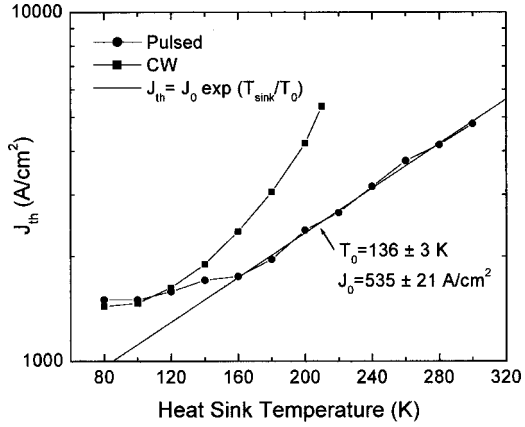

FIG. 2. Threshold current density (J_{th}) vs heat sink temperature for operation in pulsed mode (circles) and cw mode (squares). Also shown is the fit to the empirical function $J_{th}=J_0\exp(T_{sink}/T_0)$ (solid line).

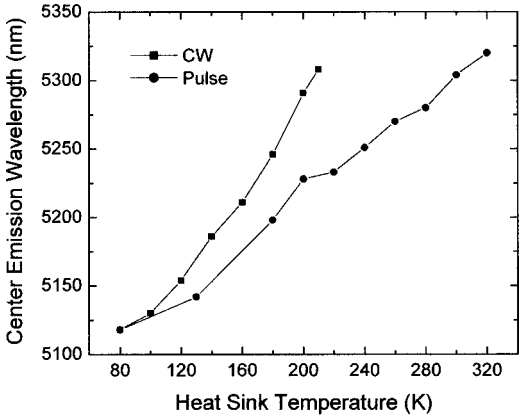

FIG. 3. Emission wavelength vs heat sink temperature under pulsed operation (circles) and cw operation (squares). Both cw and pulsed spectra were taken at a current density of $\sim 1.1 \cdot J_{th}$.

removal capacity of the cryostat. However, several $L-I$ curves were taken at low temperatures by rapidly increasing the current to a much higher level before the heat sink temperature changed significantly. By doing this, a maximum output power of more than 400 mW was measured at around 80 K.

From the $I-V$ curve shown in Fig. 1, it was found that the turn-on voltage was ~6.8 V and the series resistance of the device was ~1 Ω. The turn-on voltage is close to the theoretical minimum voltage needed to overcome the potential barriers in the active region given by

$$V_S(N)=\frac{(E_{32}+E_{21})}{e}\cdot N=7.07 \text{ V}, \tag{1}$$

where N is the number of stages in the active region and $E_{32}+E_{21}=E_{\text{photon}}+E_{\text{LO-Phonon}}=272$ meV is the energy of the photon plus phonon emitted in a single three-well vertical-transition QC stage.[7] This indicates that there is no energy loss in the funnel injector region of the QC structure. Both turn-on voltage and series resistance were found to be relatively temperature independent.

Figure 2 is a plot of threshold current density versus heat sink temperature under both cw mode and pulsed mode. The cw threshold current density was extracted from the $L-I$ curves shown in Fig. 1. The pulsed mode threshold current density was extracted from pulsed mode $L-I$ curves. The pulsed mode measurements were made with 30 ns pulses and a duty cycle of less than 0.1% to insure no significant core heating occurred.

It can be seen that the threshold current density in pulsed mode increases exponentially with heat sink temperature above 160 K and can be fit to the empirical function

$$J_{\text{th}}=J_0\exp\left(\frac{T_{\text{sink}}}{T_0}\right), \tag{2}$$

where T_{sink} is the heat sink temperature and both T_0 and J_0 are fitting parameters. The best fit is found with $J_0=535\pm 21$ Å/cm^2 and $T_0=136\pm 3$ K. This is an improvement over previously reported results[3,6] and although the underlying reason for this improvement is not known, it is suspected due to a reduced defect/impurity density in the material resulting in smaller temperature dependent losses.

It can be seen in Fig. 2 that under cw operation the threshold current density increases with temperature at a rate far greater than in pulsed operation. This is a result of the high average power dissipated in the device under cw operation causing significant core heating. The cw core temperature, T_{core}, can be determined by finding the temperature in pulsed mode that gives the same threshold current density. The thermal resistance, R_{th}, between the core and the heat sink can then be calculated using

$$R_{\text{th}}=\frac{(T_{\text{core}}-T_{\text{sink}})}{V_{\text{op}}J_{\text{th}}A}, \tag{3}$$

where T_{sink} is the cw mode heat sink temperature, V_{op} is the cw mode operating voltage at threshold, J_{th} is the cw mode threshold current density, and A is the device area. Using this technique, the thermal resistance of our device was calculated to be 10.1 ± 0.1 K/W between 180 and 210 K.

For additional verification of thermal resistance, the emission spectrum of the device was measured under cw mode and pulse mode at various heat sink temperatures. The device was operated at an injection current just above threshold, $J_{\text{op}}\cong 1.1\cdot J_{\text{th}}$ and a 1/4 meter monochromator equipped with a 150 l/mm grating and 50 μm slits was used to measure the spectra. The center emission wavelength versus heat sink temperature for both cw and pulsed mode is plotted in Fig. 3.

Assuming that the emission wavelength is only dependent upon core temperature, a similar method as described above can be used to calculate the thermal resistance. In this case, the core temperature in cw mode is determined by finding the heat sink temperature in pulsed mode that gives the same emission wavelength. Again, Eq. (3) is used to calculate the thermal resistance except J_{th} is replaced with J_{op}, the cw injection current under which the spectrum was measured. From this experiment, the thermal resistance of the device was calculated to be 9.75 ± 0.95 K/W between 180 and 210 K, in close agreement with the threshold current method.

The thermal resistance of our device is somewhat higher than that reported by Gmachl *et al.* for a similar device mounted epi down, 6.0 K/W.[4] This is in contradiction to what is expected based on the area of the device in contact with the heat sink. Therefore, the higher thermal resistance is at-

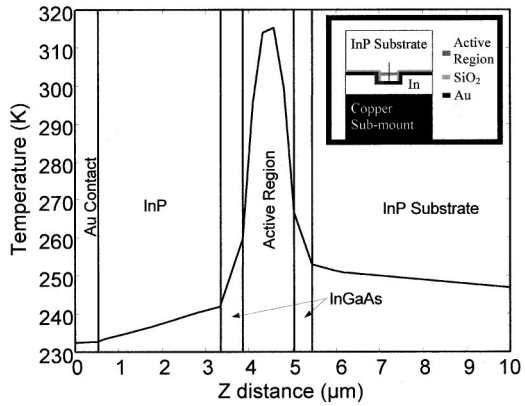

FIG. 4. Calculated temperature profile of the epi-down mounted device with 43.5 KW/cm^2 applied to the active region and the heat sink held at 210 K. The line plot is taken from the center of the 12-μm-wide cavity and shows the temperature profile starting from the Au contact, across the active region and several microns into the substrate. The inset shows a schematic (not to scale) of the structure used for the simulation. The vertical line through the center of the inverted mesa represents the region of the line plot.

tributed to the larger number of stages in the active region, 26 vs 19, and the higher temperature at which the measurement was performed, 210 vs 175 K. The thermal resistance of our device is also larger than that reported by Faist *et al.* for a device mounted epi up, ~6.6 K/W.[6] In this case, the number of stages in the active region is nearly identical, 25 vs 26, so the higher thermal resistance is attributed to a combination of the higher temperature at which the measurement was performed, 210 vs 75–95 K, and the smaller device size, 2 mm$\times$12 μm vs 3 mm$\times\sim$12 μm.

In order to gain a better understanding of the source of the thermal resistance and how it may be reduced, the theoretical temperature profile of the device was calculated by solving the two-dimensional differential equations for heat flow using finite element methods.[8] In the simulations, the power applied to the active region was 43.5 KW/cm^2 and the heat sink (bottom plane of the submount) was kept at a constant temperature of 210 K. This power density is the same power density applied to the real device at 210 K to reach threshold.

Room temperature values for thermal conductivity, as reported in the literature,[4,9,10] were used for most layers in the simulations. The thermal conductivity of the active region in the *z* direction, however, was reduced to account for the expected reduction perpendicular to the multiheterojunction structure. It was found that reducing this thermal conductivity by roughly a factor of 4 from bulk resulted in a good match of the simulated core temperature to the experimentally determined core temperature, as can be seen in Fig. 4. Further simulations showed that replacing the copper submount with chemical vapor deposition (CVD) diamond, $k=10$ W/cm K, and the SiO_2 insulating layer with a material of higher thermal conductivity, $k=100$ mW/cm K, could reduce the core temperature by roughly 13°, corresponding to a thermal resistance of 8.8 K/W.

An interesting analysis can be performed by combining Eqs. (2) and (3) and eliminating T_{core} by setting $T_{\text{sink}}=T_{\text{core}}$ in Eq. (2). One can determine that the slope of the cw threshold current density as a function of heat sink temperature reaches a limit at a heat sink temperature of

$$T_{\text{sink,max}}=T_0\left[\ln\left(\frac{T_0}{R_{\text{th}}V_{\text{op}}j_0A}\right)-1\right]. \tag{4}$$

This limit will be the effective maximum cw operating temperature.[4,6] By substituting the measured values for R_{th}, J_0, T_0, and V_{op} at 210 K into Eq. (4), it can be calculated that the maximum theoretical cw operating temperature for our device will be 212 K, in close agreement with the experimentally determined maximum operating temperature. From this it can be seen that, although our thermal resistance is higher than previously reported, the maximum cw temperature is still larger due to the high T_0 and low J_0 of our device. In addition, if the thermal resistance were lowered to 8.8 K/W, as the above simulations indicate is possible, it is calculated that the maximum cw operating temperature would reach approximately 230 K.

In conclusion, we have shown cw operation of a 5.2 μm-type I QC laser up to 210 K using epi-down mounting techniques. The device exhibited a good characteristic temperature T_0 of 136 K, a low J_0 of 535 A/cm^2, a low operating voltage V_{op} of 8.1 V, and a thermal resistance R_{th} of 10 K/W. To match the simulated temperature profile to experiment, the thermal conductivity of the active region in the *z* direction was reduced by a factor of 4 from the bulk room temperature value to 12 mW/cm K. Additional simulations indicate that the thermal resistance can be lowered to 8.8 K/W by replacing the copper submount with CVD diamond and the SiO_2 layer with a higher thermal conductivity material. This could increase the maximum cw operating temperature of the device to 230 K.

The authors would like to thank Dr. James Baillargeon and Dr. Claire Gmachl at Lucent Technologies for their helpful discussions and suggestions as well as for sharing their expertise in type I QC lasers. This work was partially sponsored by the Air Force DUST program Project No. F29601-00-2-0058 and DARPA via the University of Houston and Agreement No. 1551074/3914/K155591.

[1] M. Sigrist, *Air Monitoring by Spectroscopic Techniques* (Wiley, New York, 1994).
[2] J. Faist, C. Gmachl, F. Capasso, C. Sirtori, D. L. Sivco, J. N. Baillargeon, and A. Y. Cho, Appl. Phys. Lett. **70**, 2670 (1997).
[3] J. Faist, F. Capasso, C. Sirtori, D. L. Sivco, J. N. Baillargeon, A. L. Hutchinson, S. N. G. Chu, and A. Y. Cho, Appl. Phys. Lett. **68**, 3680 (1996).
[4] C. Gmachl, A. M. Sergent, A. Tredicucci, F. Capasso, A. L. Hutchinson, D. L. Sivco, J. N. Bailargeon, S. N. George Chu, and A. Y. Cho, IEEE Photonics Technol. Lett. **11**, 1369 (1999).
[5] D. Hoestetter, M. Beck, T. Aellen, J. Faist, U. Oesterle, M. Ilegems, E. Gini, and H. Melchior, Appl. Phys. Lett. **78**, 1964 (2001).
[6] J. Faist, A. Tredicucci, F. Capasso, C. Sirtori, D. L. Sivco, J. N. Bailargeon, A. L. Hutchinson, and A. Y. Cho, IEEE J. Quantum Electron. **34**, 336 (1998).
[7] C. Gmachl, F. Capasso, A. Tredicucci, D. L. Sivco, R. Köhler, A. L. Hutchinson, and A. Y. Cho, IEEE J. Sel. Top. Quantum Electron. **5**, 808 (1999).
[8] J. Zheng, Ph.D. thesis, University of Houston, 2000.
[9] S. A. Aliev, A. Ya. Nahelski, and S. S. Shalyt, Sov. Phys. Solid State **7**, 1287 (1965).
[10] E. F. Hockings, I. Kudman, T. E. Seidel, C. M. Schmalz, and E. F. Steigmeier, J. Appl. Phys. **37**, 879 (1966).